Pergamon

Int. J. Heat Mass Transfer. Vol. 40, No. 17, pp. 4137–4149, 1997

Printed in Great Britain
0017–9310/97 $17.00 + 0.00

PII: S0017–9310(97)00019–7

Modelling and simulation of the dynamic behaviour of a shell-and-tube condenser

T. W. BOTSCH and K. STEPHAN

Institut für Technische Thermodynamik und Thermische Verfahrenstechnik, University of Stuttgart, Pfaffenwaldring 9, 70550 Stuttgart, Germany

and

J.-L. ALCOCK and D. R. WEBB†

Department of Chemical Engineering, University of Manchester, Institute of Science and Technology, Sackville Street, Manchester M60 1QD, U.K.

(*Received* 18 *January* 1997)

Abstract—A model describing the behaviour of an industrial scale shell-and-tube condenser is presented. The model can be used under steady-state as well as under transient conditions and is able to predict vapour and condensate flow rates, pressure drop and the temperatures of the vapour, condensate, wall and coolant. The derivation of the material and energy balances is presented. Thus the apparatus is subdivided into increments corresponding to the location of the baffles in the condenser. Each of these baffle spaces is assumed to be fully mixed. The heat and material fluxes between the phases are determined using local transfer coefficients which are calculated for each baffle space. The model also includes the determination of the pressure profile along the apparatus. The results of several simulations are compared with experimental data to achieve a validation of the model. Both the steady-state and the transient behaviour of the condenser were examined, the latter when the system was subjected to step changes in each of the five key loads that determine the condenser behaviour. These are the pressure, steam flow rate, air flow rate, coolant flow rate and coolant inlet temperature. The results of the simulations agreed well with the experimental data. © 1997 Elsevier Science Ltd.

1. INTRODUCTION

In the design of a modern chemical process it has become important to satisfy high standards with regard to economy and environment. Lower energy and material input rates and lower production of waste products may be achieved by material and energy recycle streams. These may reduce production costs but the design and operation of the more complex chemical process plants that ensue, become more demanding and their transient behaviour can only be predicted by computer simulations.

These simulations require models of every single process unit to allow simulation not only of the individual apparatus, but also of the whole installation. The models must satisfy two major demands. They must be detailed enough for an accurate prediction of the time dependent behaviour of flow rates, temperatures, pressures and concentrations at the outlet of each unit, but the calculations must also be quick enough to ensure that they are faster than the real time behaviour of the system. The model of a shell-and-tube condenser presented here is consequently limited and it can be classified as being of intermediate complexity.

It appears that the transient behaviour of industrial condensers has not been examined in detail, despite its relevance to start-up, safety and process control. Work has only been carried out on the calculation of temperature and velocity fields in power plant condensers [1] as well as on investigating simple models for ideal cross flow condensers of rectangular shape [2] which are not usually validated by experimental data. In this work a model has been developed that is able to simulate the steady-state and dynamic behaviour of a condenser under conditions in which it might be found in chemical process plants. The industrial-scale shell-and-tube condenser installed in the Pilot Plant at UMIST was instrumented so that the dynamic response of the system could be measured [3]. The system studied was the condensation of steam from air under reduced pressure. The model equations were solved within the dynamic process simulation tool DIVA [4] developed in the Department of Chemical Engineering of the University of Stuttgart. A brief outline of the model and a discussion of preliminary results have already been given by the authors [5]. In the present paper the model is presented in detail, it is validated by comparing predicted and measured data,

† Author to whom correspondence should be addressed.

NOMENCLATURE

A	heat exchange area [m^2]
$\bar{C}_p$	molar heat capacity [kJ (kmol^{-1} K^{-1})]
$d_{t,i}$	inner tube diameter [m]
$d_{t,o}$	outer tube diameter [m]
D_{ik}	binary diffusivity [m^2 s^{-1}]
$\bar{H}$	molar enthalpy [kJ kmol^{-1}]
$\Delta\bar{H}^v$	latent heat of vaporization [kJ kmol^{-1}]
n	number of moles [kmol]
$\dot{N}$	molar flow rate [kmol s^{-1}]
$\dot{n}$	molar flux [kmol m^{-2} s^{-1}]
N_b	number of baffles
p	pressure [N m^{-2}]
p_s	saturation pressure [N m^{-2}]
p_i	partial pressure [N m^{-2}]
R	number of tube passes
$\mathscr{R}$	universal gas constant [kJ kmol^{-1} K^{-1}]
s	boundary layer thickness [m]
T	temperature [K]
t	time [s]
U	internal energy [kJ]
V	volume [m^3]
$\bar{V}$	molar volume [m^3 kmol^{-1}]
y	mole fraction.

Greek symbols

α	heat transfer coefficient [kJ m^{-2} s^{-1}]
β	mass transfer coefficient [kmol m^{-2} s^{-1}]
δ	film thickness [m]
τ	time constant [s]
ζ	direction perpendicular to the interface.

Subscripts

C	coolant
G	gas
I	interface
L	condensate
W	wall
i	component i
(n)	nth baffle space
(j)	jth tube pass
in	entering baffle space (n)
out	leaving baffle space (n)
0	inlet of the apparatus.

and results of simulations describing the transient behaviour of the system are discussed.

2. MODELLING

The model describes the condensation of steam from a mixture with air in a shell-and-tube condenser. Figure 1 shows the equipment to be modelled. The shell-side where the condensation takes place is divided into N_b+1 compartments by N_b vertically cut segmental baffles. The gas enters the condenser at one end and is forced by the baffles to cross the tube bundle N_b+1 times. Condensation takes place on the outside of the tubes and the condensate formed is collected at the bottom of the shell from where it flows towards the outlet because of the inclination of the unit. The tubes are cooled on the inside by cooling water, which is fed to the inlet header and traverses the equipment several times according to the number R of flow passes provided. Figure 1 shows the two pass arrangement of the cooling water found in the UMIST condenser, which is used for the validation of the model. The shell side of the condenser is divided into eight baffles spaces.

As a first step the model subdivides the condenser into the two headers and the shell where heat exchange and condensation takes place. The headers are then split into a number of separate units according to the number of flow passes provided. The further subdivision of the shell into smaller units follows the location of the baffles. Every unit then corresponds to one baffle space so that N_b+1 units have to be considered. Each baffle space contains $R+2$ control volumes, one for the gas phase, one for the condensate

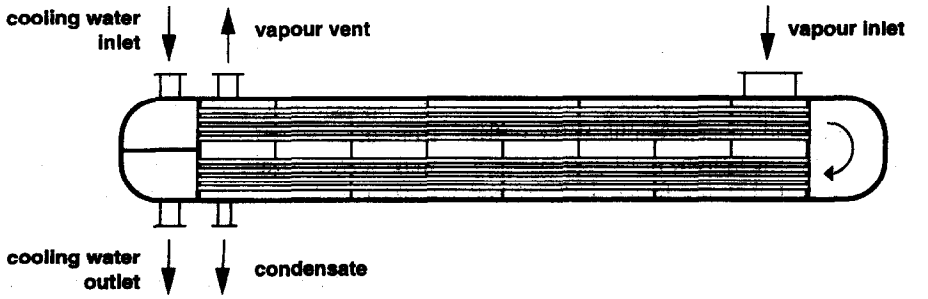

Fig. 1. Schematic presentation of a shell-and-tube condenser; the vapour inlet and the baffles are 90° rotated.

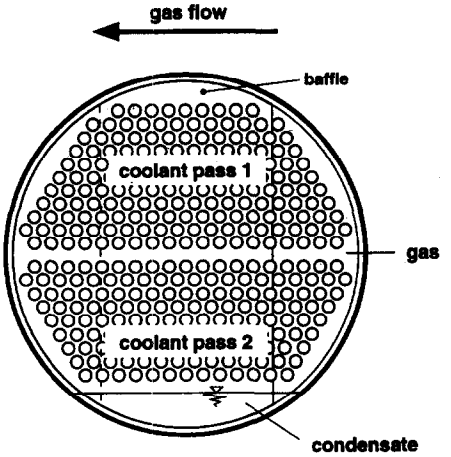

Fig. 2. Sectional view of one baffle space containing the four control units gas, condensate, coolant pass 1 and coolant pass 2.

phase and one for each coolant pass. These control volumes are shown schematically for a two pass arrangement in Fig. 2.

It is assumed that the variables of the gas phase do not change between the two coolant passes, that is the gas is fully mixed normal to the flow direction. For that reason, mean values of temperature $T_{G,(n)}$, pressure $p_{(n)}$, composition $y_{G,(n)}$ and flow rate $\dot{N}_{G,(n)}$ are used for the calculation of the physical properties of the gas phase and the heat and material transfer coefficients in the baffle space (n). The condensate in the small pools formed by the baffles at the bottom of the shell is assumed to be completely mixed and at constant temperature $T_{L,(n)}$. All other variables in any baffle space differ between the two coolant passes which determine their values. Table 1 shows the variables which depend only on the baffle space and those which are different between each coolant pass. It is clear that coolant temperature T_C, the tube wall temperature T_W and the coolant-side heat flux $\dot{q}_C$ must be different for different cooling passes. The heat flux $\dot{q}_L$ through the liquid film on the tubes depends strongly on the tube wall temperature and also influences the interfacial temperature T_I and composition y_I. Finally the heat flux $\dot{q}_G$ through the gas film and the material flux $\dot{n}$ over the interface depend on the interfacial conditions and therefore on the tube pass.

All flow rates, temperatures, concentrations and heat and mass fluxes listed in Table 1 depend on their location in the condenser and on time. Their values can be determined by solving material and energy balances for each phase. These balances will be derived in the following sections.

Figure 3 shows the control volumes in one baffle space. For the gas phase and the condensate in the shell only one control volume has to be considered for each baffle space. The balances over the other control volumes, that is the wall and the coolant and the equations describing the interface and the condensation on the tubes have to be stated separately for each tube pass. In Fig. 3 only one tube pass j is shown. Material balances have to be written for the gas phase and for the condensate in the basin at the bottom of the shell. The temperatures of the gas, the interface, the wall, the coolant and the condensate in the shell follow from energy balances over the corresponding control volumes. The model assumes that thermodynamic equilibrium at the interface gives the mole fraction y_I of the condensable component at the interface.

2.1. *Material and energy balances for the gas phase*

The terms that have to be considered in deriving the material and energy balance of the gas phase are displayed in Fig. 3. The time dependent change in the number of moles in the gas phase in one baffle space (n) follows as the difference between, the convective flows entering and leaving the volume, and the flow of the condensing species towards the interface with the summation over the number of tube passes R.

Table 1. Variables to be calculated for describing the behaviour of a shell-and-tube condenser

Variables depending only on the baffle space (n)	
$\dot{N}_{G,(n)}$	Gas flow rate
$T_{G,(n)}$	Gas temperature
$y_{G,(n)}$	Mole fraction of the condensable component in the gas
$\dot{N}_{L,(n)}$	Condensate flowrate
$T_{L,(n)}$	Condensate temperature
Variables depending on the baffle space (n) and the tube pass (j)	
$T_{C,(n,j)}$	Coolant temperature
$T_{W,(n,j)}$	Wall temperature
$T_{I,(n,j)}$	Interfacial temperature
$y_{I(n,j)}$	Mole fraction of the condensable component in the gas at the interface
$\dot{q}_{C,(n,j)}$	Heat flux from the wall to the coolant
$\dot{q}_{L,(n,j)}$	Heat flux from the interface to the wall
$\dot{q}_{G,(n,j)}$	Heat flux from the gas to the interface
$\dot{n}_{(n,j)}$	Material flux over the interface

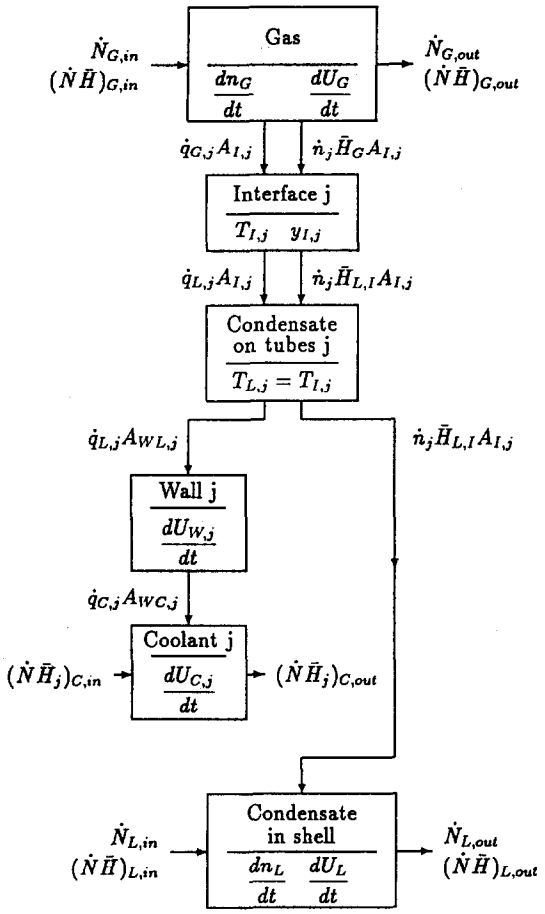

Fig. 3. Heat and material flows entering and leaving the different control units of one baffle space. Only one tube pass j is shown.

$$\frac{\partial n_{G,(n)}}{\partial t} = \dot{N}_{G,in} - \dot{N}_{G,out} - \sum_{j=1}^{R} \dot{n}_{(n,j)} A_{(n,j)}. \quad (1)$$

The number of moles $n_{G,(n)}$ in one baffle space can be expressed in terms of the geometric volume $V_{G,(n)}$ of the gas in the baffle space (n) under consideration, and the molar volume $\bar{V}_G$ of the gas. The geometric volume of the gas is assumed to be constant but the volume of the liquid pool at the bottom of the shell is neglected. This condensate volume may vary with time but is very small compared to the volume of the gas. The molar flow rates $\dot{N}_{G,in}$ and $\dot{N}_{G,out}$ are calculated as the arithmetic mean of the flowrates of the neighbouring volumes. With these assumptions the material balance for the gas phase turns out to be

$$-\frac{V_{G,(n)}}{(\bar{V}_G)^2}\frac{\partial \bar{V}_G}{\partial t} = \frac{1}{2}\dot{N}_{G,(n-1)} - \frac{1}{2}\dot{N}_{G,(n+1)} - \sum_{j=1}^{R} \dot{n}_{(n,j)} A_{(n,j)}. \quad (2)$$

The mole fraction y_G of the condensable component in the bulk of the gas in baffle space (n) follows directly from the gas flow rate $\dot{N}_{G,(n)}$ in that baffle space and the values $\dot{N}_{G,0}$ and $y_{G,0}$ at the inlet. The flow rate of the non-condensable air does not change along the condenser so that one can calculate y_G from

$$(1-y_G)\dot{N}_G = (1-y_{G,0})\dot{N}_{G,0}. \quad (3)$$

For the derivation of the energy balance of the gas phase one has to take into account the $2+2R$ terms shown in Fig. 3, the convective enthalpy flows $(\dot{N}\bar{H})_{G,in}$ and $(\dot{N}\bar{H})_{G,out}$, the enthalpies $\bar{H}_G\dot{n}_j A_{I,j}$ of the condensing fluxes and the conductive heat fluxes from the gas towards all R tube passes,

$$\frac{\partial U_G}{\partial t} = (\dot{N}\bar{H})_{G,in} - (\dot{N}\bar{H})_{G,out} - \sum_{j=1}^{R} (\dot{n}_j\bar{H}_G + \dot{q}_{G,j})A_{I,j}. \quad (4)$$

The internal energy on the left hand side of equation (4) can be replaced by the molar internal energy, the molar volume and the geometric volume of the gas balance space. The molar internal energy is then converted to the molar enthalpy and finally to the temperature. Having introduced the material balance equation (2) into equation (4) and approximating the enthalpy flows $(\dot{N}\bar{H})_{G,in}$ and $(\dot{N}\bar{H})_{G,out}$ by the arithmetic mean of the values of the neighbouring baffle spaces the energy balance of the gas phase yields,

$$V_{G,(n)}\frac{\bar{C}_{p,G}}{\bar{V}_G}\frac{\partial T_G}{\partial t} = \frac{1}{2}\dot{N}_{(n-1)}(\bar{H}_{G,(n-1)} - \bar{H}_{(n)}) + \frac{1}{2}\dot{N}_{(n+1)}(\bar{H}_{G,(n)} - \bar{H}_{(n+1)}) - \sum_{j=1}^{R} \dot{q}_{G,j}A_{I,j}. \quad (5)$$

2.2. *Material and energy balances for the condensate phase*

All condensate produced on the tube bundle within one baffle space adds to the condensate in the basin at the bottom of the shell leading to an increasing condensate flow rate. The condensate material balance follows as

$$\frac{\partial n_{L,(n)}}{\partial t} = \dot{N}_{L,in} - \dot{N}_{L,out} + \sum_{j=1}^{R} \dot{n}_{(n,j)} A_{(n,j)}. \quad (6)$$

The number of moles $n_{L,(n)}$ can again be calculated from the molar volume of the condensate and the geometric volume $V_{L,(n)}$ of the liquid filled region. This geometric volume, in contrast to that of the gas balance space, varies with time. It equals the hold up between two baffles which is strongly influenced by the condensate flow rate itself. The higher the condensate flow rate, the greater the depth of the liquid in the pools of condensate needed to cause flow over the weirs formed by the baffles. Therefore two equations have to be added to determine the condensate level and the geometric volume of the condensate in each baffle space. The liquid level can be calculated approximately as a function of the condensate flow rate [6], and the geometric volume of the condensate then follows from the geometry of the condenser and the liquid level.

The condensate pools are assumed to be completely mixed, so that they may be modelled as continuous stirred tanks. Hence the flow leaving each condensate pool has the same properties as the upstream pool, $\dot{N}_{in} = \dot{N}_{(n-1)}$ and $\dot{N}_{out} = \dot{N}_{(n)}$.

Knowing the geometric volume $V_{L,(n)}$ of the condensate pool between two baffles, the material balance of the condensate can be rewritten as,

$$\frac{1}{\bar{V}_L}\frac{\partial V_{L,(n)}}{\partial t} - \frac{V_{L,(n)}}{(\bar{V}_L)^2}\frac{\partial \bar{V}_L}{\partial t} = \dot{N}_{L,(n-1)} - \dot{N}_{L,(n)} + \sum_{j=1}^{R} \dot{n}_{(n,j)} A_{(n,j)}. \quad (7)$$

When deriving the energy balance of the condensate one has to take three terms into account, the convective enthalpy flows entering and leaving the balance space and the enthalpy of the condensate which is produced on the tubes of the bundle and which drains to the condensate pool in the shell. The temperature of the condensate on the tubes of each tube pass is assumed to be equal to the corresponding interfacial temperature so that the energy balance of the condensate turns out to be

$$\frac{\partial U_L}{\partial t} = (\dot{N}\bar{H})_{L,in} - (\dot{N}\bar{H})_{L,out} + \sum_{j=1}^{R} (\dot{n}\bar{H}_{L,I})_{(n,j)} A_{(n,j)}. \quad (8)$$

As before, the internal energy of the condensate is expressed in terms of pressure, temperature and geometric volume and further the material balance equation (2) can be introduced into equation (8). The convective flows $(\dot{N}\bar{H})_{L,in}$ and $(\dot{N}\bar{H})_{L,out}$ have the same properties as the baffle space they leave so that the final energy balance over the condensate in the shell follows as

$$V_{L,(n)}\frac{C_{p,L}}{\bar{V}_L}\frac{\partial T_L}{\partial t} - p\frac{\partial V_{L,(n)}}{\partial t} = \dot{N}_{(n-1)}(\bar{H}_{(n-1)} - \bar{H}_{(n)}) + \sum_{j=1}^{R} (\dot{n}(\bar{H}_{L,I})_{(n,j)} - \bar{H}_{(n)}) A_{(n,j)}. \quad (9)$$

2.3. *Interfacial conditions*

The temperature and the mole fraction of the condensable component at the interface must be known for the determination of the heat and mass fluxes. The interfacial temperature is calculated from an energy balance over the interface.

$$\dot{q}_L = \dot{q}_G + \dot{n}\Delta\bar{H}^{v*} \quad (10)$$

The interface cannot accumulate energy so that the difference between the heat fluxes $\dot{q}_L$ through the liquid film on the tubes and $\dot{q}_G$ from the gas to the interface must equal the heat released during condensation of vapour at a molar flux $\dot{n}$. The heat of vaporization $\Delta\bar{H}^{v*}$ used in equation (10) combines the latent and the sensible heats to cool the gas from T_G to T_I.

$$\Delta\bar{H}^{v*} = \bar{C}_{p,G}(T_G - T_I) + \Delta\bar{H}^{v} \quad (11)$$

The model assumes thermodynamic equilibrium at the interface. Hence the mole fraction of the condensable component at the interface can be determined as a function of the total pressure p and the saturation pressure of the condensable component at the interfacial temperature T_I.

$$y_I = \frac{p_s(T_I)}{p} \quad (12)$$

2.4. *Material and energy fluxes*

The flux of the condensing component i always consists of a diffusive and a convective part.

$$\dot{n}_i = J + y\dot{n}_t \quad (13)$$

The diffusive part J is caused by a concentration gradient and can be evaluated by Fick's law. In the case examined of one single condensable component the material flux $\dot{n}_i$ equals the total flux $\dot{n}_t$ over the interface so that equation (13) can be transformed into

$$\dot{n}_i = -\frac{p}{\mathscr{R}T} D_{12}\frac{\partial y}{\partial \zeta} + y\dot{n}_i, \quad (14)$$

where D_{12} is the binary diffusivity and ζ is a coordinate perpendicular to the interface. With the definition of a mass transfer coefficient

$$\beta_{12} = \frac{p}{\mathscr{R}T}\frac{D_{12}}{s} \quad (15)$$

one can solve equation (14) to give the Colburn–Hougen equation [7],

$$\dot{n} = \beta_{12} \ln\left(\frac{1-y_I}{1-y_G}\right) \quad (16)$$

for the determination of the material flux $\dot{n}$ of the condensable component over the interface. The mass transfer coefficient β_{12} can be determined from the gas-side heat transfer coefficient by analogy [8].

Three heat fluxes have to be determined when solving the model equations. These are the heat flux from the gas to the interface, the one through the condensate film and the coolant-side heat flux. The gas-side heat flux, which has to be transferred from the gas to the interface and which causes the sensible cooling of the gas, is calculated as

$$\dot{q}_G = \alpha_G \frac{\Phi_T}{e^{\Phi_T} - 1}(T_G - T_I). \quad (17)$$

It appears as the product of the temperature driving force and the heat transfer coefficient α_G modified for mass transfer. The term $\Phi_T/(e^{\Phi_T}-1)$, first introduced by Ackermann [9], takes into account the influence of the mass transfer upon the simultaneous heat transfer. The parameter Φ_T is the ratio of the sensible gas cooling from T_G to the interfacial temperature T_I and the heat flux $\dot{q}_G$. It is defined as

$$\Phi_T = \frac{\dot{n}_t \bar{C}_{p,G}}{\alpha_G}. \quad (18)$$

The gas side heat transfer coefficient α_G is identified as the single phase heat transfer coefficient for the same geometry and may be calculated according to standard correlations given in the VDI–Wärmeatlas [10].

The heat flux $\dot{q}_L$ through the condensate film on the tubes follows from the temperature difference between the interface and the wall as

$$\dot{q}_L = \alpha_L (T_I - T_w). \quad (19)$$

The heat transfer coefficient α_L used in equation (19) is given in Ref. [11] as a superposition of a shear stress controlled and a gravity controlled heat transfer coefficient. It is corrected in the model by inclusion of the heat transfer resistances of the wall and of the dirt layer on it. The coolant-side heat transfer coefficient, required for calculating $\dot{q}_C$, is taken from the VDI–Wärmeatlas [10].

2.5. *Energy balances for wall and coolant*

An energy balance over the wall is necessary for the inclusion of the effect of heat accumulation in the tubes of the condenser during unsteady conditions. It is derived as,

$$\rho_W \frac{\pi}{4} d_{t,o}^2 c_W \frac{\partial T_w}{\partial t} = \dot{q}_L \pi d_{t,o} - \dot{q}_C \pi d_{t,i}. \quad (20)$$

This equation includes the specific density ρ_W and the specific heat capacity c_W of the tube material and inner and outer diameters $d_{t,i}$ and $d_{t,o}$.

The terms to be considered when deriving the energy balance for the coolant are shown in Fig. 3. These are the convective enthalpy flows $\dot{N}\bar{H}_{in}$ and $\dot{N}\bar{H}_{out}$ and the heat flux transferred through the tube wall. After expressing the internal energy in terms of temperature, pressure and the geometric volume $V_{C,(n)}$ and approximating the enthalpy flows by the arithmetic means of the values of the neighbouring control spaces, the energy balance of the coolant results.

$$V_{C,(n)} \frac{\bar{C}_{p,C}}{\bar{V}} \frac{\partial T_C}{\partial t} = \frac{1}{2} \dot{N}_C (\bar{H}_{C,(n-1)} - \bar{H}_{C,(n+1)}) + \dot{q}_C A_C. \quad (21)$$

2.6. *Pressure drop*

The pressure in the shell of the condenser strongly influences the saturation temperature of the vapour and consequently the temperature driving force and the heat flux over the interface. It is therefore essential to have an exact knowledge of the pressure profile over the equipment. This is calculated following the method of Bell, as given by Taborek in [12]. The pressure drop consists of two major parts, the so-called crossflow pressure drop occurring when the fluid crosses the tube bundle and the window pressure drop in the baffle clearance where the gas changes its direction. In addition to these two parts the model also includes an accelerational pressure drop to account for the decrease of gas velocity when the vapour condenses, an Ackerman-type-correction for the influence of the mass flux of condensation on the pressure drop and a two-phase correction factor, accounting for the influence of condensate flow, which may be dispersed or stratified.

3. NUMERICAL TREATMENT

The material and energy balances presented in Section 2 are formulated as time-dependent partial differential equations. Apart from these the model consists of many algebraic equations describing the heat and mass fluxes, the pressure drop, the mole fractions and all the physical properties which are calculated as a function of temperature, pressure and composition for every control volume. Thus the model leads to a system of algebraic and time-dependent partial differential equations (DAE–system).

The numerical solution of the system was carried out within the dynamic process simulation environment DIVA [4, 13] which has been developed in the Department of Chemical Engineering of the University of Stuttgart. DIVA is a flow sheet orientated tool for the dynamic simulation of chemical process plants comprising many unit operations. Hence the model implemented for a shell-and-tube condenser can be used not only for the simulation of the dynamic behaviour of a free standing single condenser but also for the simulation of a whole process plant including shell-and-tube condensers in conjunction with other unit operations.

4. RESULTS

The usefulness of the model was assessed by a large number of simulations. Comparisons with experimental data validated the model for both the steady-state and dynamic conditions. The experiments were performed at UMIST in Manchester [3]. In the following sections these comparisons are presented and the steady-state and transient behaviour of the apparatus is examined.

4.1. *Condensation under steady-state*

The pressure drop across one baffle space depends on the gas velocity at that location which itself is a function of the local molar flow rate. In condensation processes, the molar flow rate decreases along the apparatus because of the removal of the condensable component. The correlation used for the heat transfer therefore has a strong influence on the calculated pressure drop. Hence for a validation of the pressure drop correlation, one must compare the predicted pressure profile with experimental data obtained from a single-phase heat exchanger. For that reason a number of gas cooling experiments were performed in which the condenser was fed with hot air only. These exper-

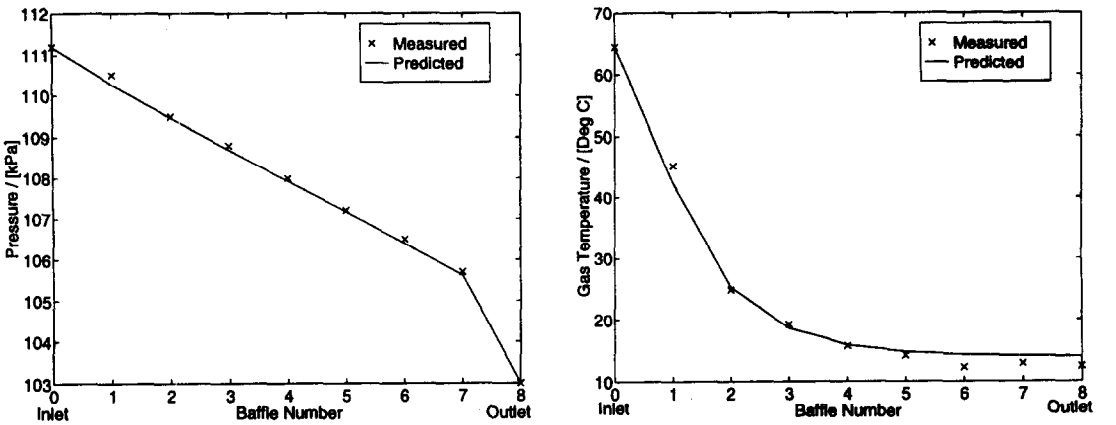

Fig. 4. Comparison of predicted and measured pressure and gas temperature profiles over the condenser when it is operated as single phase heat exchanger and fed with hot air.

iments were carried out with the outlet at atmospheric pressure and the measured pressure and gas temperature profiles were compared with the results of the corresponding simulations.

Figure 4 displays the measured and the predicted gas temperature and pressure profiles of one typical run. The inlet conditions of the particular run were an air load of 25 mol s^{-1}, an inlet gas temperature of 65.21°C, a cooling water flow rate of 0.69 kmol s^{-1} and a cooling water temperature of 13.7°C. The pressure drop is the same over all baffle spaces. It is a function of the geometry of the apparatus and the local gas velocity which depends mainly on the gas flow rate. The influence of the changing gas temperature on the density and consequently on the gas velocity is taken into account in the calculations but is found to be very small in that there is an almost constant pressure drop in the first seven baffle spaces. A noticeably higher pressure drop occurs between the last baffle and the outlet. This is caused by the pressure drop in the outlet nozzle which has to be added to the pressure drop in the last baffle space. The pressure drop in the inlet nozzle is very small compared to that in the outlet because of the larger diameter of the inlet nozzle. The pressure profile over the whole length of the apparatus including the two nozzles is well predicted. The model also calculates the gas temperature accurately, indicating that the single-phase heat transfer coefficients for the gas- and the coolant-sides are correctly determined.

A large number of condensation experiments were carried out and used for the further validation of the model. The ranges of the inlet conditions of these experiments are given in Table 2. The table also highlights two runs which will be discussed in detail. The steam feed was in all experiments super-heated and its inlet temperature was always about 105°C. When comparing the measured and the predicted gas temperatures, it was found that the calculated value was always much higher than the measured one at and close to the inlet. The predicted gas bulk temperature decreased only slowly as the gas flow moved along the condenser whereas the measured temperature dropped sharply over the first baffle space and based on predictions the gas was saturated from baffle 1 onwards. This quick cooling of the super-heated gas is probably due to the entrainment of many condensate droplets into the gas flow. These droplets have a lower temperature than the gas and lead to a large additional heat transfer area cooling the super-saturated gas down to its saturation temperature. This process of heat exchange between the gas and the condensate droplets is not taken into account in the energy balance of the current model in the gas phase. Although the sensible heat transfer has a strong influence on the gas temperature, it can be neglected compared to the latent heat transferred from the gas to the tube wall. The effect was considered by calculating the saturation temperature of the gas during the simulation and using this value for the comparison with the experimental data. The saturation temperature of the gas

$$T_{sat} = T_{sat}(p_i) \tag{22}$$

depends on the partial pressure p_i which itself can be

Table 2. Values of the inlet variables

Variable	Minimum	Maximum	Run 1	Run 2	Unit
Steam flow rate $\dot{N}_s$	6	20	19	16	mol s^{-1}
Air load $\dot{N}_A$	0.25	1.6	1	0.28	mol s^{-1}
Pressure p	7	62	38	14	kPa
Cooling water flow rate $\dot{N}_C$	680	1330	1130	1300	mol s^{-1}
Cooling water temperature T_C	25	34	31.6	29.8	°C

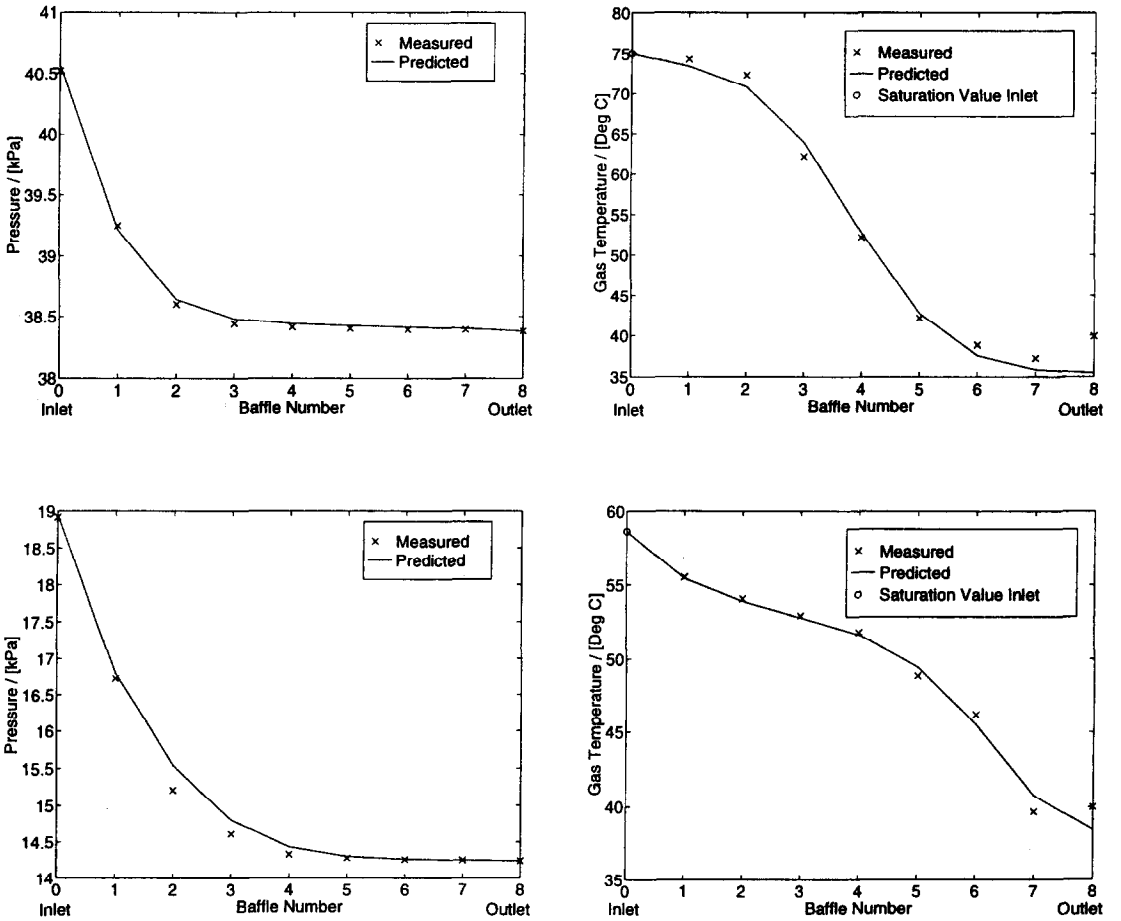

Fig. 5. Comparison of predicted and measured pressure and gas temperature profiles over the condenser. The upper diagrams show run 1, the lower diagrams represent run 2. The inlet conditions of both runs can be taken from Table 2.

determined by Dalton's law as $p_i = y_G p$ from the total pressure p and the steam mole fraction y_G in the bulk of the gas.

The measured and the calculated pressure and saturation temperature profiles are shown for two typical runs in Fig. 5. The inlet conditions for these two runs are given in Table 2. Run 1, shown in the upper half of the figure, is typical of operating conditions where only a small part of the heat exchanger surface is needed for the condensation of the vapour. The pressure drop is highest over the first two baffle spaces which indicates that the bulk of the condensation takes place there. Further downstream the pressure profile is flatter signifying that most of the vapour has already condensed and that mainly air cooling occurs in this region. The good agreement in the pressure profile shows the accuracy of the model as it indicates that both the gas flow rate and the local condensation rates are correctly predicted. This is particularly pleasing because, with $\Delta p \propto u^{1.8}$, pressure drop is very sensitive to flow.

Clearly the correct prediction of the pressure profile is only significant when the pressure drop is relatively high. As can be seen from the figure, this is only the case close to the inlet, where high gas flow rates are still present. Further downstream the gas flow rate is so small that significance is lost. Nevertheless, the model can prove its usefulness in that region, by an accurate prediction of the saturation temperature of the gas, of which measured and calculated values are shown for run 1 in the upper half on the right hand side of Fig. 5. The measured and the predicted saturation temperature do not decrease within the first two baffle spaces although the pressure sharply decreases in that region. This is due to the high mole fraction of steam in the inlet gas. Even though most of the condensation has taken place close to the inlet of the apparatus, the steam mole fraction does not decrease significantly. The mole fraction and hence the saturation temperature only decrease when most of the steam has already condensed so that the amount of non-condensing species is of the same order of magnitude as the remaining vapour. The accurate prediction of the saturation temperature is therefore a good indication of the application of the model in the region, where the right prediction of the pressure profile is not as meaningful. The marked difference between the measured and predicted temperatures at the outlet

arises because the model does not account for the geometry of the condenser at this point. In the condenser the vapour flows across, and is influenced preferentially by, the warmest coolant pass because the vapour outlet nozzle is situated on the top of the condenser. In the model the temperature is calculated as if the vapour follows the same path as in all the other baffle spaces and is equally influenced by both coolant passes, i.e. as though the outlet nozzle was located at the centre-line.

The second run, of which the results are shown in the lower part of Fig. 5, is characterized by a lower pressure and therefore a smaller temperature driving force. Consequently more of the heat exchanger surface is required for the condensation of the steam. Pressure drop is highest at the beginning and has significant values in the first four baffle spaces. Only in the very last part of the apparatus is the pressure profile almost flat indicating that comparatively little steam is present in the gas flow. This indicates that the main condensation rate takes place in the first four baffle spaces. The steep gradient in saturation temperature, indicating the location of the condensation front, occurs further downstream compared to run 1 because of the lower material flux over the interface. Further, the saturation temperature close to the inlet of the condenser decreased more steeply than it did in run 1. This is because of the lower pressure, which gives the pressure drop a stronger influence on the change in saturation temperature. The temperature at the outlet is again badly predicted because of the outlet geometry of the test condenser which is not taken into account by the model.

Comparisons of calculated and experimental data were not only carried out for the two cases presented but for a large number of additional runs. Figure 6 compares the calculated and measured overall pressure drop for all runs of the present study. The condensation experiments are displayed by crosses whereas circles represent the air cooling runs. It can be seen that the discrepancy in predicting the overall pressure drop is less than 10% for most runs with air-steam mixtures as well as for those using only hot air. The dependence of pressure drop on $u^{1.8}$ would imply that flow rates in condensation are predicted within $\pm 5\%$. The pressure and saturation temperature profiles of most runs also agree well with the experimental

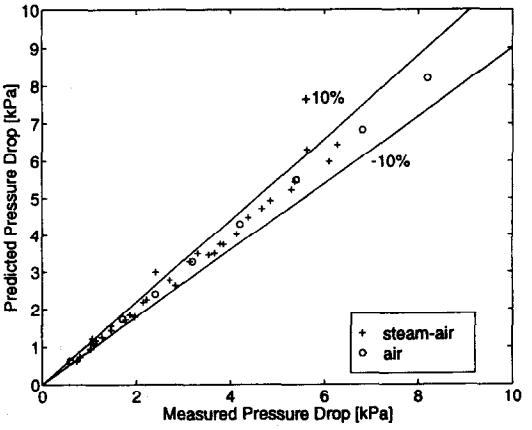

Fig. 6. Comparison of predicted and measured pressure drop over the condenser. The circles represent air cooling experiments, the crosses stand for condensation runs.

values, indicating that the local condensation rates and therefore the distribution of the gas flow rate and the steam mole fraction is accurately predicted by the model. All comparisons showed a good prediction of the steady-state behaviour of the shell-and-tube condenser.

4.2. *Dynamic behaviour of the apparatus*

The dynamic behaviour of the system was examined by imposing a step change in turn to each of the five key loads that determine the condenser behaviour. The values of these five variables before and after the step change are shown in Table 3. All step changes were imposed in both directions ensuring reproducible experimental results. In the following the transient behaviour of the system after a step change in pressure and a step change in steam flow rate will be discussed.

The change in any of the key variables was imposed by opening or closing a valve. Although this was carried out automatically, an ideal step could not be realized because of the finite time required for the movement of the valve. Similarly an ideal step-function should not be used as input for the simulation. It was rather found that the measured change of the inlet variable Y is better reproduced by an exponential function of form,

Table 3. Overview over the keyloads of the systems and how they were changed for the dynamic experiments and simulations

	Step change in					
	Steam flow rate $\dot{N}_s$	Air load $\dot{N}_A$	Pressure p	Cooling water Flow rate $\dot{N}_C$	Cooling water Temperature T_C	
$\dot{N}_s$	10.28 ↔ 16.67	12.94	11.11	11.16	11.17	mol s^{-1}
$\dot{N}_A$	0.284	0.286 ↔ 1.155	0.271	0.285	0.282	mol s^{-1}
p	14.1	45.5	13.6 ↔ 40.5	14.1	14.1	kPa
$\dot{N}_C$	1283	1230	1283	1076 ↔ 1282	1283	mol s^{-1}
T_C	32.1	36.3	36.0	32.1	25.1 ↔ 29.1	°C

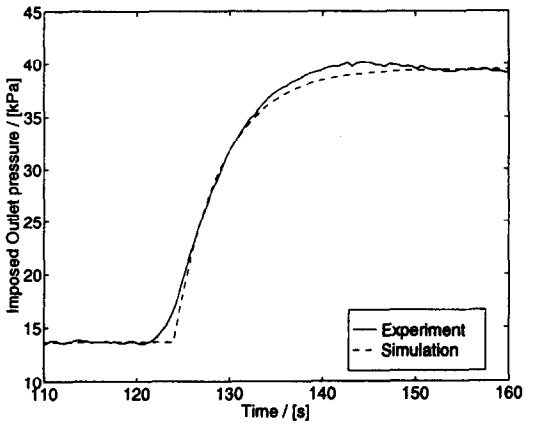

Fig. 7. Imposed step change in pressure. The solid line represents the measured values, the dashed line stands for the exponential function which was imposed to the model.

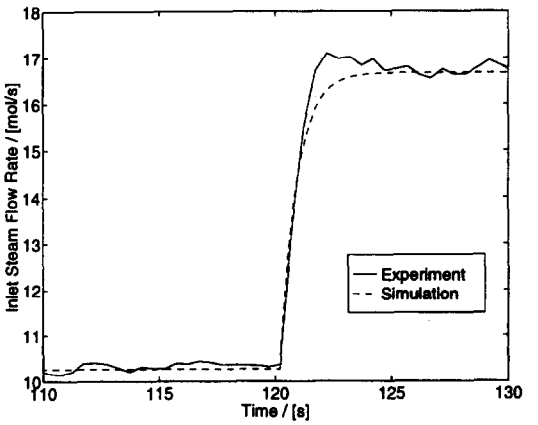

Fig. 8. Imposed step change in steam flow rate. The solid line represents the measured values, the dashed line stands for the exponential function which was imposed to the model.

$$Y = Y_0 + \Delta Y\left(1 - \exp\left(\frac{t}{\tau} - \frac{t_0}{\tau}\right)\right) \qquad (23)$$

in which Y_0 is the value before the step, ΔY the height of the step, t_0 the time when the change starts and τ the time constant of the exponential function. Figures 7 and 8 show experimentally measured variations of the two key variables, outlet pressure and inlet flow rate, that were imposed to the experimental system for measuring the response. The figures also display the functions approximating the measured variations which were used as input for the dynamic simulations. Experimentally the change in pressure could only be imposed relatively slowly and the time constant of the corresponding exponential function was found to be 5 s. In contrast the change in steam flow rate proceeded faster leading to a time constant of 0.7 s.

Figure 9 shows the response of the actual gas temperatures and the predicted saturation temperatures at different locations along the condenser to an increase in condenser outlet pressure from 13.85 to 39.42 kPa. The other operating parameters can be read from Table 3. The increase of the outlet pressure leads to a higher pressure in the system which produces a higher saturation temperature and hence a higher temperature driving force. Consequently the condensation front in the apparatus moves upstream as less of the heat exchanging surface is required for condensing the fed steam.

It can be seen from Fig. 9 that the actual new steady-state is characterized by a higher gas temperature opposite the first two baffles and a lower one at the other locations compared to the conditions before the change in pressure. The temperature opposite the baffles near the inlet increase because of the increasing pressure which brings about a higher saturation temperature. This higher saturation temperature in the inlet region gives a higher temperature driving force so that more steam is condensed in the first baffle spaces after the change in pressure. Consequently the mole fraction of the steam in the baffle spaces downstream becomes smaller, the partial pressure decreases and therefore the saturation temperature at those positions decreases.

The mechanism is clarified in Fig. 10 which shows calculated profiles of the steam mole fraction at different times during and after the change in pressure. The time-difference between adjacent profiles is $\Delta t = 0.5$ s. It can be seen that the mole fraction was reduced to an outlet value of 0.4 when the condenser was operated at low pressure. The decrease in the steam mole fraction proceeded relatively slowly remaining above 0.9 for the first three baffle spaces and reached its highest gradient only in the fifth baffle space. After the change to a higher pressure, the mole fraction is seen to decrease to a much lower outlet value of 0.14. The highest gradient, indicating the location of the condensation front, moved upstream to the third baffle space. The figure shows that the mole fraction changed by less than 25% in the first two baffles, but by more than 60% over the downstream locations. Hence, the change in mole fraction only dominated the partial pressure, and consequently the gas temperature, at locations close to the outlet, whereas the gas temperature in the first two baffle spaces was mainly controlled by the changing total pressure.

It can be seen from Fig. 9 that the model satisfactorily predicts the effects of the pressure increase with the first two temperatures increasing and the rest decreasing. The steady-state values before and after the change are predicted as accurately as the transient behaviour during the change. The only noticeable discrepancies in the two steady-state profiles are the old steady-state temperature opposite baffle 6 and the new steady-state temperature opposite baffle 3, which is in both cases close to the location of the condensation front. In the latter case the temperature profile over the exchanger is very steep in that region so that a small error in the prediction of the position of the

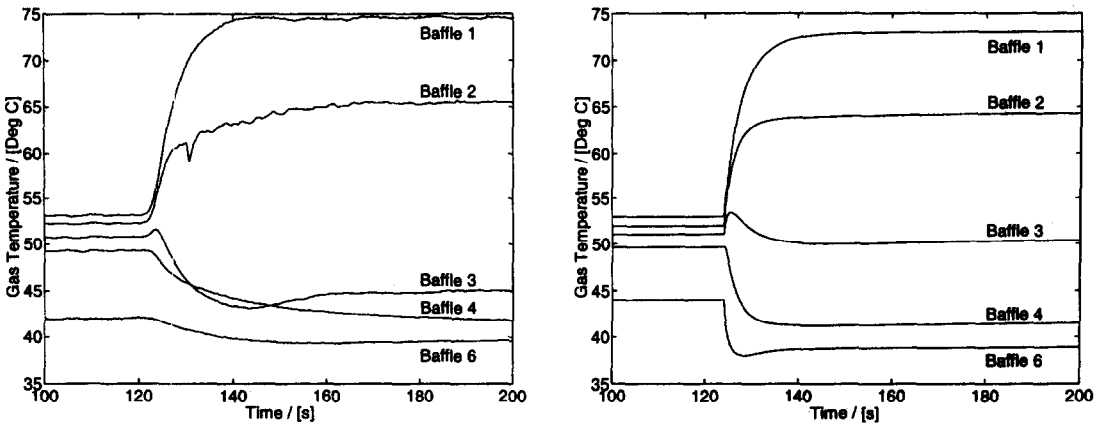

Fig. 9. Transient response of the gas temperature opposite baffles 1–4 and 6 after a step increase in pressure. The left diagram shows the measured values, the right one the calculated saturation temperatures.

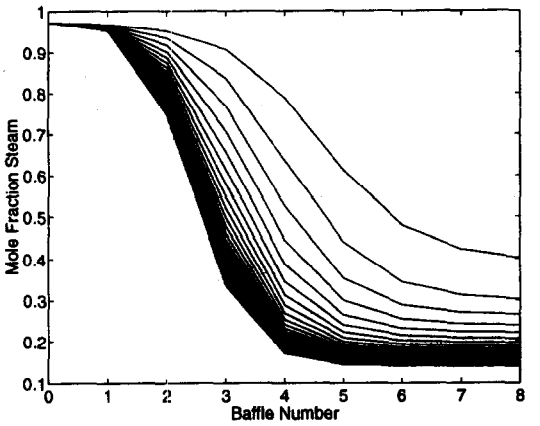

Fig. 10. Steam mole fraction profiles over the condenser at different times after the step increase in pressure. The time difference between the shown profiles is $\Delta t = 0.5$ s.

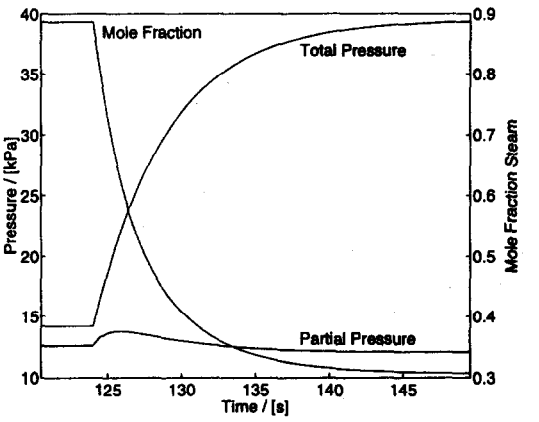

Fig. 11. Variation of the total pressure p, the steam mole fraction y_G and the partial pressure p_i with time at baffle 3. The increasing total pressure and the decreasing steam mole fraction influence the partial pressure such that it peaks during the first seconds after the change.

condensation front leads to a comparatively large error in the predicted temperature.

The predicted response times are shorter than those of the experiment, a discrepancy which becomes larger the closer the examined temperature is to the outlet. This is probably caused by the thermal inertia of the condenser. In the model only the heat capacity of the tube bundle is taken into account, but not that of the shell or baffles.

The model proves its worth in predicting the small peak in gas temperature opposite baffle 3, which occurs as the condensation front moves to the third baffle space from further downstream. The mechanism leading to this effect is explained in Fig. 11 which displays the transient responses of the total pressure, the steam mole fraction and the partial pressure at the position examined. During the first few seconds, when the saturation temperature increases, the partial pressure at baffle 3 is more strongly influenced by the increasing total pressure than by the decreasing mole fraction. When the partial pressure and the saturation temperature have reached their maxima, the mole fraction has only decreased by 25%

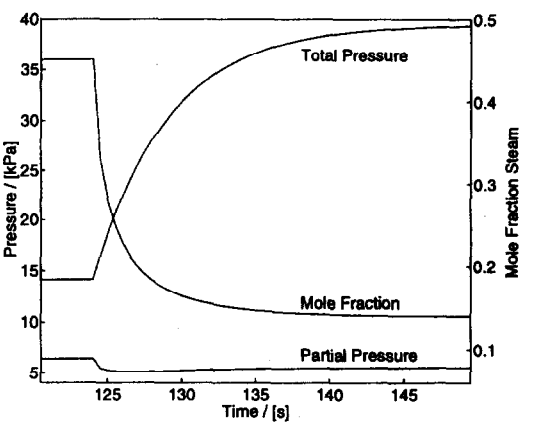

Fig. 12. Transient responses in the total pressure p, the steam mole fraction y_G and the partial pressure p_i at baffle 6. The partial pressure decreases in the first seconds after the change in outlet pressure to a value which is smaller than the new steady-state one.

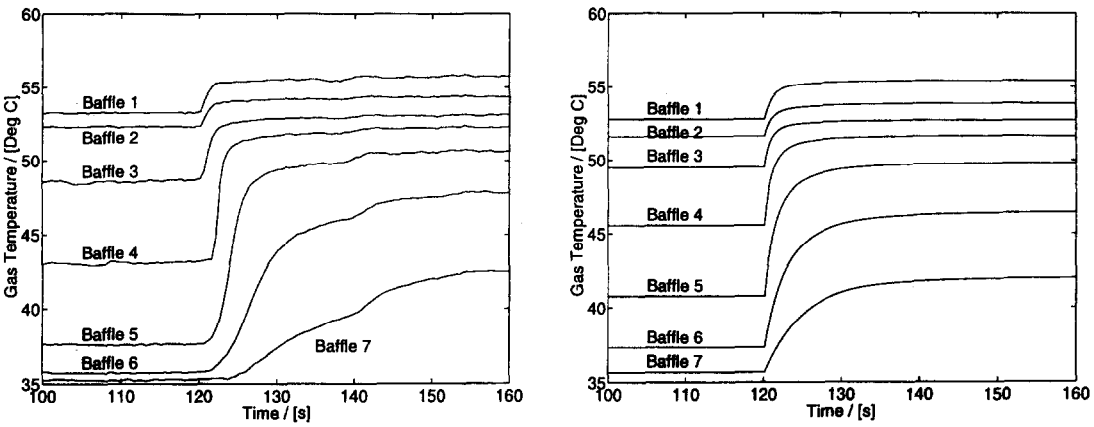

Fig. 13. Transient response of the gas temperature opposite baffles 1–6 after a step increase in steam flow right. The left diagram shows the measured temperatures, the right one the calculated values.

to 0.65 while the total pressure has already increased by 50% to more than 20 kPa. Afterwards the partial pressure decreases as the mole fraction decreases further and its influence becomes stronger than that of the total pressure.

The same mechanism leads to the minimum in the predicted saturation temperature opposite baffle 6. The total pressure at this location responds in almost the same way as that at baffle 3, but the change of the mole fraction proceeds at a lower level. This causes the mole fraction to dominate the partial pressure in the first seconds whereas the increasing total pressure later causes the partial pressure to recover, Fig. 12. The calculated saturation temperature is determined by the partial pressure and consequently behaves in the same way. This predicted minimum is not observed because it is dominated by the effect of the equipment's thermal inertia which is not fully taken into account by the model. An effect similar to that described for saturation temperature at baffle 6 could be, together with the energy accumulation, the reason for the measured cross-over of the two temperatures opposite baffles 3 and 4.

The measured and predicted responses of the saturation temperatures at different locations in the condenser to a step increase in steam flow rate are shown in Fig. 13. After the increase in steam flow rate more heat exchanger area is required and therefore the condensation front moves downstream. Because more steam is fed to the system, the mole fraction at every location in the condenser becomes higher, increasing the local partial pressure and leading to a higher saturation temperature of the gas. It can be seen from the figure that the model correctly predicts the system response to the increase in steam flow rate. The original steady-state temperatures opposite baffle 4 and 5 are overpredicted, indicating that the calculated position of the condensation front was not exactly right. The response times are again somewhat underpredicted, especially those of the temperatures in the downstream part of the apparatus, the region which is at last affected by changing inlet conditions. It is again clear that the calculated response times in that region become too short if the model does not fully include the equipment's thermal inertia.

5. CONCLUSIONS

The steady-state and the transient behaviour of a shell-and-tube condenser have been modelled. The condenser is subdivided into smaller units defined by the location of the baffles. Every baffle space is modelled as a number of control volumes which are assumed to be fully mixed. Material and energy balances were derived for each of these control volumes and heat and material fluxes between the shell side and the coolant were calculated using correlations from the literature. The model is of intermediate complexity so that it can be used for simulation of the dynamic behaviour of a single condenser or a whole process plant.

The model was validated by a comparison with experimental data obtained from an industrial-sized condenser at UMIST. Steady-state temperature and pressure profiles were compared for many different inlet conditions including the use of the exchanger for single phase gas cooling only. The success in predicting the steady-state behaviour indicates that the spatial divisions are sufficient to allow for axial mixing effects.

The dynamic behaviour of the system was examined in five different experiments, each corresponding to a step change in one of the five key loads. The results were also compared with experimental data. The model is able to predict the effects of a change in each of the five key loads on the saturation temperatures in the equipment. Measured effects including fine structure such as the small peak in the time-dependent saturation temperature were predicted and can be explained. Problems in predicting the response times

of the temperatures close to the outlet of the condenser are probably due to the failure to account for some of the thermal inertia of the condenser.

Acknowledgements—The authors gratefully acknowledge the financial support provided by the Deutsche Forschungsgesellschaft (DFG) in a research project 'Methoden zur Modellierung und Berechnung der Dynamik verfahrenstechnischer Prozesse' and the financing of the expenses of the joint visits by the British Council and the Deutscher Akademischer Austauschdienst (DAAD).

REFERENCES

1. Al-Sanea, S., Rhodes, N., Tatchell, D. G. and Wilkinson, T. S., A computer model for detailed calculation of the flow in power station condensers. In *Condensers: Theory and Practice*, IChemE Symposium Series no. 75, 1983, pp. 70–75.
2. Ciechanowicz, W., The dynamics of a vapor condenser. *Nuclear Engineering and Design*, 1968, **7**, 1–8.
3. Alcock, J.-L., Webb, D. R., Botsch, T. W. and Stephan, K., An experimental investigation of the dynamic behaviour of a shell-and-tube condenser. *International Journal of Heat and Mass Transfer*, 1997, **40**, 4129–4135.
4. Kröner, A., Holl, P., Marquart, W. and Gilles, E. D., DIVA—an open architecture for dynamic simulation. *Computers in Chemical Engineering*, 1990, **14**, 1289–1295.
5. Alcock, J.-L., Botsch, T. W., Stephan, K., Stevenson, R. W. and Webb, D. R., The transient behaviour of a shell-and-tube condenser. In *Proceedings of the 4th U.K. National Conference on Heat Transfer*, Manchester. Mechanical Engineering Publications 1995, pp. 341–345.
6. Truckenbrodt, E., *Fluidmechanik Band 1: Grundlagen und elementare Strömungsvorgänge dichtebeständiger Fluide*, 2nd edn. Springer, Berlin, 1980, p. 748f.
7. Colburn, A. P. and Hougen, O. A., Design of cooler-condensers for mixtures of vapours with condensing gases. *Industrial Engineering Chemistry*, 1934, **26**, 1178–1182.
8. Chilton, T. H. and Colburn, A. P., Mass transfer coefficients, prediction from data on heat transfer and fluid friction. *Industrial Engineering Chemistry*, 1934, **26**, 1183–1187.
9. Ackermann, G., Wärmeübergang und molekulare Stoffübertragung im gleichen Feld bei großen Temperatur- und Partialdruckdifferenzen. *VDI-Forschungsheft*, 1937, **382**, 1–16.
10. Gnielinski, V., Wärmeübertragung bei erzwungener einphasiger Strömung. *VDI-Wärmeatlas*, 7th edn, Chapter G. VDI, Düsseldorf, 1994.
11. Blangetti, F. and Krebs, R., Filmkondensation reiner Dämpfe. VDI-Wärmeatlas, 7th edn, Chapter Ja. VDI, Düsseldorf, 1994.
12. *Heat Exchanger Design Handbook*, Chapter 3.3. Hemisphere, Washington, DC, 1983.
13. Helget, A. and Gilles, E. D., Dynamische Prozeß- und Anlagensimulation. In *Prozeßsimulation*, ed. H. Schuler. DECHEMA-VCH, 1994, pp. 109–148.